LETTERS

Striations, duration, migration and tidal response in deep tremor

Satoshi Ide[1]

Deep tremor in subduction zones is thought to be caused by small repeating shear slip events on the plate interface with significant slow components[1–4]. It occurs at a depth of about 30 kilometres and provides valuable information on deep plate motion and shallow stress accumulation on the fault plane of megathrust earthquakes. Tremor has been suggested to repeat at a regular interval[1,2], migrate at various velocities[4–7] and be modulated by tidal stress[6,8,9]. Here I show that some time-invariant interface property controls tremor behaviour, using precise location of tremor sources with event duration in western Shikoku in the Nankai subduction zone, Japan. In areas where tremor duration is short, tremor is more strongly affected by tidal stress and migration is inhibited. Where tremor lasts longer, diffusive migration occurs with a constant diffusivity of $10^4\,m^2\,s^{-1}$. The control property may be the ratio of brittle to ductile areas, perhaps determined by the influence of mantle wedge serpentinization on the plate interface. The spatial variation of the controlling property seems to be characterized by striations in tremor source distribution, which follows either the current or previous plate subduction directions. This suggests that the striations and corresponding interface properties are formed through the subduction of inhomogeneous structure, such as seamounts, for periods as long as ten million years.

One of the most important discoveries in Earth science in the last decade is that of deep non-volcanic tremor[1] often accompanied with a slow slip event. The combined phenomena have come to be known as episodic tremor and slip[2]. In western Shikoku, in the Nankai subduction zone, Japan, most seismically observed tremor and geodetically observed slow slip events share a common mechanism—shear slip on the plate interface[10,11]—and a scaling law in which the event duration is proportional to the seismic moment (that is, the spatial integral of slip multiplied by the rigidity)[12]. Similar phenomena have been discovered in other subduction zones[13,14], and tremor appears to occur as shear slip on the plate interface at least in Nankai, Cascadia and Costa Rica[15], although there is still ongoing debate on the precise location of tremor relative to the plate interface[14].

Here I focus on tremor in western Shikoku. Tremor in this area has been proposed to be repeating small low-frequency earthquakes[4], each of which occurs as slip on the plate interface based on both the planar distribution of hypocentres[3] and the focal mechanism of low-angle thrust type[11]. A high ratio of compressional (P)-wave velocity to shear (S)-wave velocity (v_P/v_S) around the tremor sources determined by seismic tomography implies the existence of water at high pore pressure[3,16]. High-speed tremor migration of up to 10 km in 10 minutes (about $10\,m\,s^{-1}$) was also first discovered here[4]. Other categories of slow earthquakes, very-low-frequency earthquakes[5] and slow slip events[10] have been studied here as well. Here, I reveal the fine internal structure of this well-studied tremor zone by determining tremor source locations and durations.

The data are the velocity seismograms recorded at 23 stations of Hi-net, the high-sensitivity seismograph network maintained by the National Research Institute for Earth Science and Disaster Prevention, Japan, for five years from April 2004 to March 2009 (Fig. 1). I divided continuous data into half-overlapping 300-s time windows and determined the location of the tremor source, if it existed, for each time window. The hypocentre determination method is an envelope correlation method[1,17]. This method has been widely used to determine the location of tremor phenomena, but has been thought to include significant errors, particularly in depth. However, it can be an effective location method, provided it is accompanied by appropriate processing to reduce the influence of outliers, as detailed in the Methods. In addition to the locations, I estimated the source duration using the stacked envelope aligned with the wave arrival time from the source location. The event duration is defined as the period for which the amplitude exceeds half of the maximum.

Figure 1 shows the locations of tremor sources and stations. For most events, the standard deviation of location determined by the least squares solution is less than 1 km, vertically and horizontally, which is probably underestimated. I can constrain the actual location error to some extent using ordinary earthquakes. I apply the envelope correlation method without eliminating ordinary earthquakes. 95% of ordinary earthquakes larger than magnitude one ($M > 1$) in the catalogue of the Japan Meteorological Agency (JMA) were also detected and located by the envelope correlation method. The estimated depths of these ordinary earthquakes are systematically shallower by about 1.2 km (with a standard deviation of 4.5 km) than those in the JMA catalogue. The epicentres are better constrained, with a standard deviation of about 1.5 km (see the Methods). I take these figures as representative of typical errors in my analysis. These ordinary earthquakes are not shown in Fig. 1, because it includes only events with duration longer than 10 s.

Despite errors of about 5 km in depth, the shape of tremor source distribution clearly shows northwestward-dipping planes, with increasing dip angles from east (A) to west (C) (see Fig. 1). The result is consistent with the previous location of low-frequency earthquakes in this area[3,15], but the resolution is insufficient to discuss whether this pattern represents a single plane. At the western end of the tremor zone, the depth may be a little deeper owing to systematic errors in depth, as demonstrated in the Supplementary Information. The relatively high dip angle in this region cannot be explained by this error. Except for the depth of this region, the depth distribution and the spatial pattern of dip angle changes are consistent with the depth of the oceanic Mohorovičić discontinuity (Moho) estimated using receiver functions[18].

Many lineaments within the tremor can be identified, as shown by the arrows in Fig. 1. Their orientation clusters in one of two directions: either N 55° W or N 22° W. The former is the direction of current plate motion[19] and the latter is approximately the direction

[1]Department of Earth and Planetary Science, University of Tokyo, Hongo 7-3-1, Bunkyo, Tokyo 113-0033, Japan.

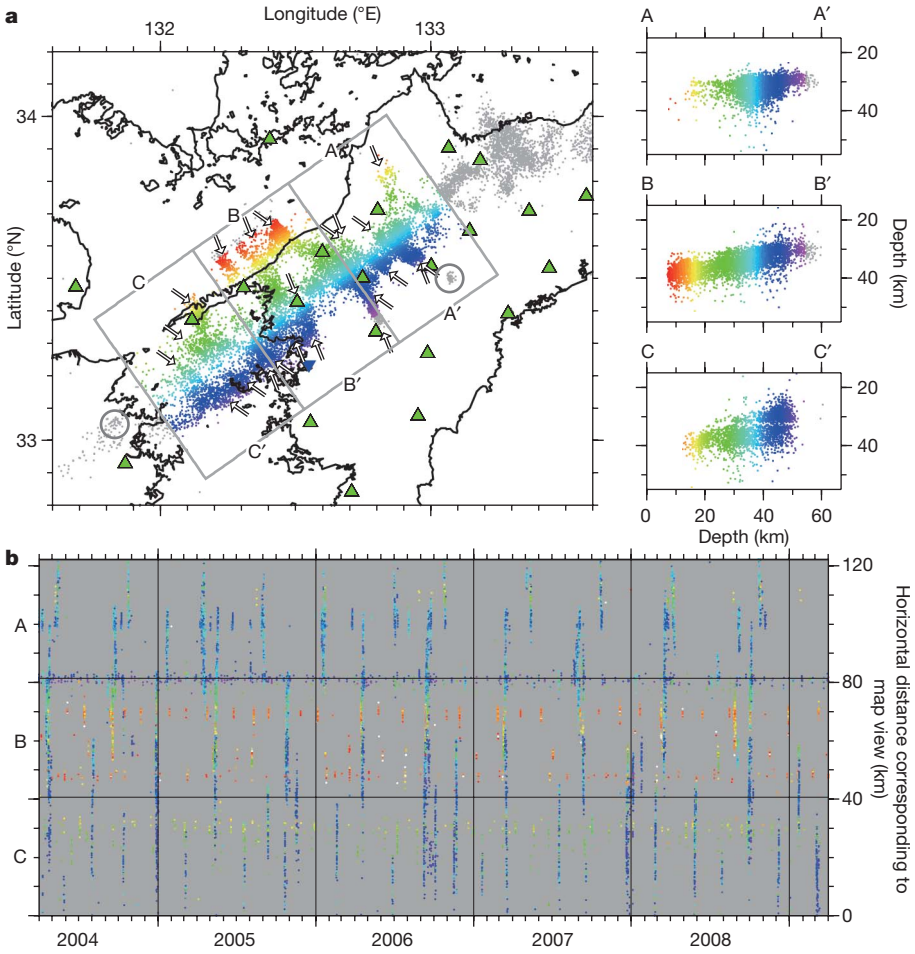

Figure 1 | Distribution of tremor sources having durations longer than 10 s. **a**, Map view (left panel) and three cross-sections (right panels) for the grey rectangular region. Sources in the box are coloured according to the location in the N 40° W direction, and sources outside the box are grey. Green triangles are Hi-net stations and the blue triangle is the Uwajima tide station. Two grey open circles indicate explosion events in quarries. Arrows are aligned in either N 55° W or N 22° W directions. **b**, Space-time plot of tremor sources for five years. Colours are as in the top panels.

of the past plate motion before 3–5 million years ago, when the direction of subduction of the Philippine Sea plate suddenly changed from NNW to WNW[20,21]. This suggests that these lineaments are formed by relative plate motion—both previous and current, just as micro-earthquake streaks are observed to follow the slip direction along the creeping section of the San Andreas Fault, California[22].

The time-location plot of tremor sources (Fig. 1) shows that large tremor activity repeats at a time interval of 3–6 months, as found previously[23]. Some small clusters repeat at much shorter intervals of 1–2 months, or last almost continuously, such as the purple cluster at the boundary between A and B. The intervals seem to be characteristic for each cluster, which suggests they are controlled by some local property of the plate interface.

Tremor distribution in Fig. 1 is substantially different from the distribution of low-frequency earthquakes detected by the JMA[24] (Fig. 2a). These low-frequency earthquakes are identified as isolated events in tremor sequences. Therefore, the event duration must be very short. If I select short events with durations between 10–15 s, the distribution (Fig. 2b) is similar to that of low-frequency earthquakes. This distribution is essentially the same as the recently discovered double-peak alignments of tremor activity at the shallow and deep parts of the tremor zone[25]. On the other hand, the distribution of events with durations between 100–300 s (Fig. 2b) is quite different, and spatially complementary. This means that the event duration is also controlled by some local property of the interface. Figure 2c shows the typical duration measured by the median duration, which has a consistent pattern: the short-duration events are peripheral to, and surround, areas of long duration. There are several circular holes near the centre of the tremor zone where no tremor was detected. Because the typical duration is long near these holes, it is possible that there are still longer slip events that are undetected by our analysis.

The same local property seems to control the sensitivity to tidal loading. Tremor can be modulated by tidal stress[6,8,9], but Fig. 2d shows that does not apply at all locations. I measure sensitivity to tidal stress using the normalized Fourier spectral amplitude, as described in the Methods. Although in some areas tremor occurs quite periodically at the semidiurnal principal lunar (M2) period, there are also wide areas without such correlation. By comparing Fig. 2c and d, in general tremor can be seen to be sensitive to tidal stress where short events occur. In other words, in such areas tremor is easily activated by external load but terminates quickly. Tremor may generate longer slip that is less sensitive to external load in an area where long events occur.

Tremor duration or sensitivity to tidal stress can control overall tremor behaviour. If tremor occurs without tidal modulation in an area where event duration is long, tremor often shows clear diffusive migration, in which the migration time is equal to the square of distance divided by the diffusivity. Figure 3a and b shows such examples. Tremor is slightly controlled by the tide, but migrates even when the tidal stress is in the opposite sense. A parabolic curve assuming the diffusivity of $10^4\,m^2\,s^{-1}$ is almost always a good approximation. Diffusion has been considered as a possible mechanism of tremor[12,26], but the migration is not always clearly diffusive. Figure 3c and d shows examples in which migration is not clear. In such cases, tremor occurs only when the tide level is high and migration is inhibited.

As shown above, there is some local property controlling event duration, periodicity, sensitivity to tidal stress and diffusive migration.

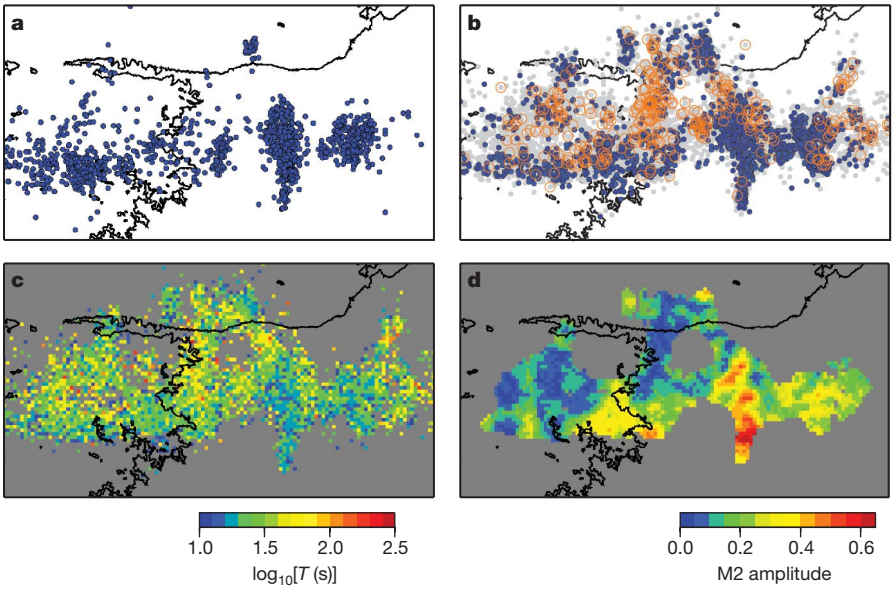

Figure 2 | Distribution of low-frequency earthquakes and tremor sources with duration and sensitivity to the tidal stress. **a**, Distribution of low-frequency earthquakes determined by the JMA. The area in the rectangular box in Fig. 1 is shown. **b**, The distribution of tremor sources is shown by grey circles. Those with duration T between 10 and 15 s and exceeding 100 s are shown by blue circles and orange circles, respectively. **c**, Spatial distribution of median duration estimated in each 1-km^2 cell. **d**, Sensitivity to the tidal stress estimated using the amplitude of the normalized Fourier spectrum at the semidiurnal principal lunar (M2) period of 12.420601 h.

What is it? Slow earthquakes may occur as a combination of brittle earthquake-like slip and ductile slower slip. In the deeper part of the plate interface, shear motion must be ductile, but in shallower areas a certain part of the interface is brittle. A tremor zone may be an area where a slow slip interface is pinned by numerous small brittle patches. The density of brittle patches could be the local property. Rupture of patches activates slow motion, but the amount of activated slow motion may be spatially variable. For dense patch distribution, only a small slow slip area is activated and the slow slip duration is short. Conversely, if the distribution is sparse, large slow motion can be activated around each patch and grows to some critical size, above which slow slip may break brittle patches without the help of tidal stress. In this case, a feedback system between slow slip and brittle patches produces a diffusive slip event, which is less controlled by tidal stress.

The duration is short along the shallowest edge of the tremor zone, where a clear lineament along strike suggests a drastic change of material property. This line may correspond to the Moho discontinuity, where dehydration reaction and serpentinization of the stagnant wedge mantle are likely to begin[27,28], as suggested by the structural seismic surveys in the Tokai region, Japan[29]. Serpentinization requires water transport along the subducting plate, which may be enhanced along with subducting irregularities such as seamounts. In the Nankai subduction zone, a subducting seamount near the trough has been identified by a structural survey[30]. Many similar seamounts must have subducted along the plate interface in the past and some of them may have survived through the shallower locked section where megathrust earthquakes occur. Some of them subducted in the direction of N 22° W before 5 million years ago, whereas others have subducted or are subducting in the direction of N 55° W. I suggest that the current lineaments shown in Fig. 1 are the record of previous seamount subduction, as summarized in Fig. 4. Similar lineaments are also visible in other tremor zones along the Nankai and the Cascadia[7] subduction zones, suggesting that it is a fundamental

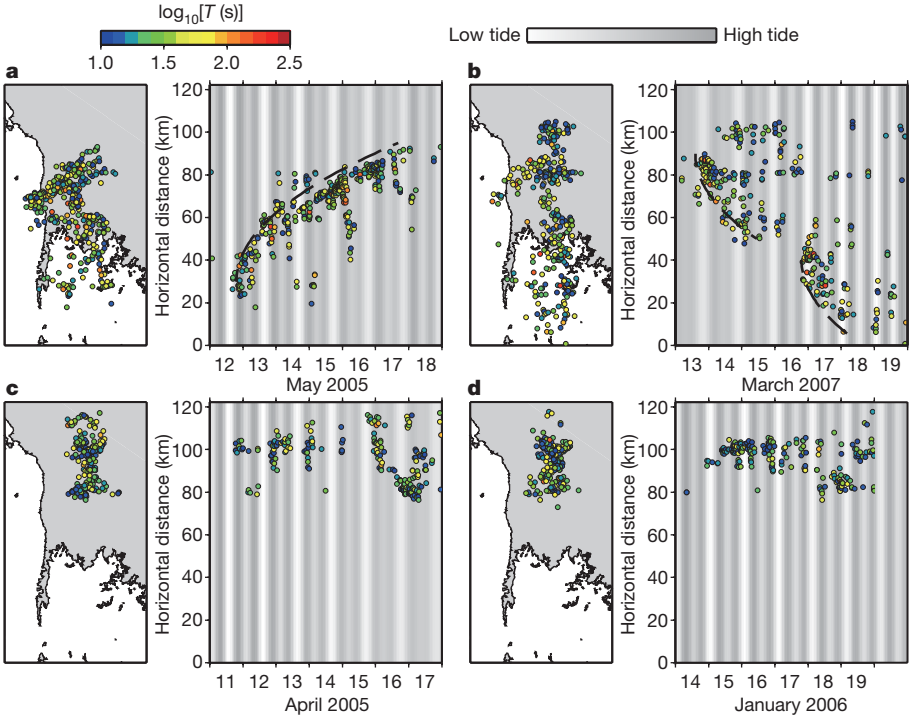

Figure 3 | Map views and space-time plots of tremor sources for active periods of one week. The area in the rectangular box in Fig. 1 is shown in the map view. Each space-time plot shows observed sea level at Uwajima station (Fig. 1) shaded in white to grey (normalized for each period). Coloured circles show the log duration. **a**, **b**, Tremor migration occurs almost continuously along a dashed parabola calculated using the diffusion coefficient of 10^4 m^2 s^{-1}. **c**, **d**, Migration is not clear. Tremor occurs mainly when sea level is high.

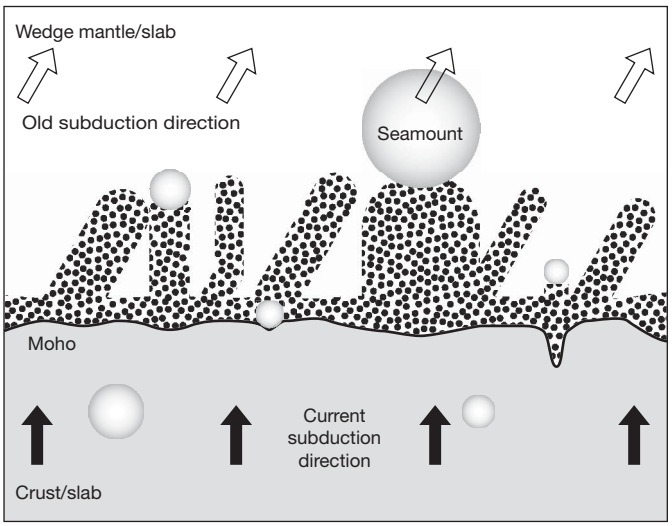

Figure 4 | Schematic illustration of plate subduction and formation of tremor zone. Guided by irregularities such as seamounts, the wedge mantle is serpentinized down to some depth. A change of subduction direction is visible as striations, shown by the dotted areas in the tremor zone.

process for tremor zones, and applicable to many other subduction zones.

METHODS SUMMARY

The hypocentre determination is based on an envelope correlation method: the envelope is ground-velocity bandpass-filtered between 2 and 8 Hz, squared, low-pass filtered below 0.3 Hz, and resampled at one sample per second, in two horizontal directions. Continuous envelope records are divided into 300-s windows. For each window, I seek a pair of envelopes, for which the maximum cross-correlation exceeds 0.6. For these pairs, I find an initial estimate of epicentral location that maximizes the number of station pairs with the same signs of difference in travel time and epicentral distance. The time difference at the maximum cross-correlation for each pair of envelopes is used as data. The data are compared with the difference of calculated S-wave arrival times based on a one-dimensional velocity structure. The best estimation of the hypocentre is given by minimizing the errors between the observed and calculated travel time differences using the Levenberg–Marquardt method. Although I determine a hypocentre for each time window, I discard the result in cases where the number of data points is smaller than 100, or the standard deviation of error is larger than a second. By comparison with the hypocentre catalogue of JMA (Supplementary Fig. 1), I estimate the standard deviation of the location to be about 1.5 km horizontally and 4.5 km vertically.

For the estimation of sensitivity to tidal stress, I prepare a circle centred at one point on the map to include 100 tremor epicentres. If the radius is smaller than 5 km, I consider a sequence of delta functions located at all hypocentral times. I calculate the amplitude of its Fourier spectrum at the semidiurnal principal lunar (M2) period, which is shown in Fig. 2d.

Full Methods and any associated references are available in the online version of the paper at www.nature.com/nature.

Received 28 March; accepted 1 June 2010.

1. Obara, K. Nonvolcanic deep tremor associated with subduction in southwest Japan. *Science* **296,** 1679–1681 (2002).
2. Rogers, G. & Dragert, H. Episodic tremor and slip on the Cascadia subduction zone: the chatter of silent slip. *Science* **300,** 1942–1943 (2003).
3. Shelly, D. R., Beroza, G. C., Ide, S. & Nakamula, S. Low-frequency earthquakes in Shikoku, Japan, and their relationship to episodic tremor and slip. *Nature* **442,** 188–191 (2006).
4. Shelly, D. R., Beroza, G. C. & Ide, S. Non-volcanic tremor and low-frequency earthquake swarms. *Nature* **446,** 305–307 (2007).
5. Ito, Y., Obara, K., Shiomi, K., Sekine, S. & Hirose, H. Slow earthquakes coincident with episodic tremors and slow slip events. *Science* **315,** 503–506 (2007).
6. Shelly, D. R., Beroza, G. C. & Ide, S. Complex evolution of transient slip derived from precise tremor locations in western Shikoku, Japan. *Geochem. Geophys. Geosyst.* **8,** Q10014 (2007).
7. Ghosh, A. *et al.* Tremor bands sweep Cascadia. *Geophys. Res. Lett.* **37,** L08301, doi: 10.1029/2009GL042301 (2010).
8. Nakata, R., Suda, N. & Tsuruoka, H. Non-volcanic tremor resulting from the combined effect of Earth tides and slow slip events. *Nature Geosci.* **1,** 676–678 (2008).
9. Rubinstein, J. L., Rocca, M. L., Vidale, J. E., Creager, K. C. & Wech, A. G. Tidal modulation of nonvolcanic tremor. *Science* **319,** 186–189 (2008).
10. Hirose, H. & Obara, K. Repeating short- and long-term slow slip events with deep tremor activity around the Bungo channel region, southwest Japan. *Earth Planets Space* **57,** 961–972 (2005).
11. Ide, S., Shelly, D. R. & Beroza, G. C. The mechanism of deep low frequency earthquakes: further evidence that deep non-volcanic tremor is generated by shear slip on the plate interface. *Geophys. Res. Lett.* **34,** L03308, doi: 10.1029/2006GL028890 (2007).
12. Ide, S., Beroza, G. C., Shelly, D. R. & Uchide, T. A scaling law for slow earthquakes. *Nature* **447,** 76–79 (2007).
13. Schwartz, S. Y. & Rokosky, J. M. Slow slip events and seismic tremor at circum-pacific subduction zones. *Rev. Geophys.* **45,** RG3004, doi: 10.1029/2006RG000208 (2007).
14. Rubinstein, J. L., Shelly, D. R. & Ellsworth, W. L. in *New Frontiers in Integrated Solid Earth Sciences, International Year of Planet Earth* 287–314 (Springer Science and Business Media, 2010).
15. Brown, J. R. *et al.* Deep low-frequency earthquakes in tremor localize to the plate interface in multiple subduction zones. *Geophys. Res. Lett.* **36,** L19306, doi:10.1029/2009GL040027 (2009).
16. Matsubara, M., Obara, K. & Kasahara, K. High-VP/VS zone accompanying non-volcanic tremors and slow-slip events beneath southwestern Japan. *Tectonophysics* **472,** 6–17 (2009).
17. Maeda, T. & Obara, K. Spatio-temporal distribution of seismic energy radiation from low-frequency tremor in western Shikoku, Japan. *J. Geophys. Res.* **114,** B00A09, doi: 10.1029/2008JB006043 (2009).
18. Shiomi, K., Obara, K. & Sato, H. Moho depth variation beneath southwestern Japan revealed from the velocity structure based on receiver function inversion. *Tectonophysics* **420,** 205–221 (2006).
19. Miyazaki, S. & Heki, K. Crustal velocity field of southwest Japan: Subduction and arc-arc collision. *J. Geophys. Res.* **106,** 4305–4326 (2001).
20. Seno, T. & Maruyama, S. Paleogeographic reconstruction and origin of the Philippine Sea. *Tectonophysics* **102,** 53–84 (1984).
21. Takahashi, M. Tectonic development of Japanese Islands controlled by Philippine Sea plate motion. *J. Geog.* **115,** 116–123 (2006).
22. Rubin, A. M., Gillard, D. & Got, J.-L. Streaks of microearthquakes along creeping faults. *Nature* **400,** 635–641 (1999).
23. Obara, K. & Hirose, H. Non-volcanic deep low-frequency tremors accompanying slow slips in the southwest Japan subduction zone. *Tectonophysics* **417,** 33–51 (2006).
24. Katsumata, A. & Kamaya, N. Low-frequency continuous tremor around the Moho discontinuity away from volcanoes in the southwest Japan. *Geophys. Res. Lett.* **30,** doi: 10.1029/2002GL015981 (2003).
25. Obara, K., Tanaka, S. & Maeda, T. Reevaluation of nonvolcanic tremor activity based on the hybrid method. *Eos* **90** (Fall Meet. Suppl.), abstr. T11C–1835 (2009).
26. Ide, S. A Brownian walk model for slow earthquakes. *Geophys. Res. Lett.* **35,** L17301, doi: 10.1029/2008GL034821 (2008).
27. Hyndman, R. D. & Peacock, S. M. Serpentinization of the forearc mantle. *Earth Planet. Sci. Lett.* **212,** 417–432 (2003).
28. Wada, I., Wang, K., He, J. & Hyndman, R. D. Weakening of the subduction interface and its effects on surface heat flow, slab dehydration, and mantle wedge serpentinization. *J. Geophys. Res.* **113,** B04402, doi: 10.1029/2007JB005190 (2008).
29. Kato, A. *et al.* Variations of fluid pressure within the subducting oceanic crust and slow earthquakes. *Geophys. Res. Lett.* doi: 10.1029/2010GL043723 (in the press).
30. Kodaira, S., Takahashi, N., Nakanishi, A., Miura, S. & Kaneda, Y. Subducted seamount imaged in the rupture zone of the 1946 Nankaido earthquake. *Science* **289,** 104–106 (2000).

Supplementary Information is linked to the online version of the paper at www.nature.com/nature.

Acknowledgements I thank G. C. Beroza for many useful comments. Comments from K. Wang and discussions with S. Yoshioka, T. Hori, B. Shibazaki, R. Ando and A. Namiki were helpful. This work is supported by JSPS KAKENHI (20340115) and MEXT KAKENHI (21107007). The figures were prepared using the Generic Mapping Tool (P. Wessel and W. H. F. Smith, 1998).

Author Information Reprints and permissions information is available at www.nature.com/reprints. The author declares no competing financial interests. Readers are welcome to comment on the online version of this article at www.nature.com/nature. Correspondence and requests for materials should be addressed to S.I. (ide@eps.s.u-tokyo.ac.jp).

METHODS

Hypocentre determination method. The original records are horizontal-velocity discretized at 100 samples per second. The records are bandpass-filtered between 2 and 8 Hz, squared, low-pass filtered below 0.3 Hz, and resampled at one sample per second. The square root of the resampled data is the 'envelope' I use for hypocentre determination. I use envelopes in two horizontal directions separately at 23 stations. Continuous envelope records are divided into 300-s windows, successively overlapped by 150-s.

For each window, I first seek correlated envelopes. If the maximum cross-correlation between envelopes at a station pair exceeds the assumed threshold (0.6 in this study), the two envelopes are judged to be correlated and the corresponding lag time is the travel-time difference between two stations. The difference must not exceed the travel-time difference of a horizontally propagating S-wave at the surface. With a relatively low threshold such as 0.6, even noise often correlates well. Since least-squares methods are susceptible to non-Gaussian observations, that is, outliers, some preprocessing is necessary. I adopt a robust epicentral location method that maximizes the number of station pairs that have the same sign for difference in travel time and epicentral distance. For the estimated epicentre, a datum point is judged to be an outlier when (1) the arrival time at the distant station is earlier by more than 3 s, or (2) the travel-time difference is greater by 3 s than the travel time of the slowest wave between two stations. The threshold 3 s is another control parameter that I chose by trial and error.

After removing outliers, travel-time difference data Δt_{ij} between station i at $\mathbf{x}_i$ and station j at $\mathbf{x}_j$ are used to make an observation equation:

$$\Delta t_{ij} = T(\mathbf{x}_i, \mathbf{x}_0) - T(\mathbf{x}_j, \mathbf{x}_0) + \mathbf{e}$$

where $T(\mathbf{x}, \mathbf{y})$ represents the travel time of an S-wave between $\mathbf{x}$ and $\mathbf{y}$. I calculate travel times assuming a one-dimensional velocity structure based on the tomography result of ref. 3. In fact, the difference of the assumed velocity structure affects the epicentre distribution very little. $\mathbf{x}_0$ is the hypocentre to be estimated. Assuming that $\mathbf{e}$ is the Gaussian error leads to a nonlinear least-squares minimization:

$$\mathrm{Res} = \Sigma[\Delta t_{ij} - (T(\mathbf{x}_i, \mathbf{x}_0) - T(\mathbf{x}_j, \mathbf{x}_0))]^2$$

I linearize this problem and solve it using the Levenberg–Marquardt method. For this nonlinear problem the selection of the initial parameters may affect the result. Therefore, I use the estimated epicentre and seven different initial depths—2, 5, 10, 20, 30, 50 and 100 km—and find the solution that minimizes Res. Once the solution is obtained, I calculate the standard deviation of data. If a data residual is more than three times the standard deviation, I remove it and restart the Levenberg–Marquardt method. This process is iterated until there are no removed data points.

Thus I obtain the catalogue of hypocentres estimated for each time window. Some hypocentres are not unique because time windows overlap. I search a pair of hypocentres that occurred within 40 km and 10 s, and removed the one with the larger standard deviation. I also removed poorly estimated hypocentres in cases where the number of data points is not many, smaller than 100, or the standard deviation is larger than 1 s.

Comparison of hypocentres with the JMA catalogue. My method is applicable not only to tremor, but also to ordinary earthquakes. I compare my result with the hypocentre catalogue of JMA. Supplementary Fig. 1 shows the result of comparison. Corresponding events are connected by lines. Generally, the epicentre is similar, with a minor systematic error and a standard deviation of about 1.5 km. The vertical error is a little larger, 4.5 km, and my hypocentral estimate is systematically shallower by about 1 km than that of the JMA. The difference is mostly due to the difference of assumed velocity structure. Moreover, the vertical error has a spatial pattern in that the error is larger at the edge of the network. Therefore, we should be careful not to interpret the hypocentral depth near the edge of the network. Nevertheless, considering the fact that my method uses only S-waves, the consistency between two catalogues is remarkable and the resultant hypocentral catalogue is useful for this analysis.

Estimation of sensitivity to tidal stress. For each point separated at intervals of 2 km in the box area of Fig. 1, I estimated the sensitivity of tremor activity to tidal stress as follows. I prepare a circle centred at one point on the map to include 100 tremor epicentres. If the radius is smaller than 5 km, I consider a sequence of delta functions located at all hypocentral times, t_j. I calculate the amplitude of its Fourier spectrum at the semidiurnal principal lunar (M2) period, $\omega_{M2} = 12.420601$ h, normalized by the number of events $N (= 100)$, which is:

$$\frac{1}{N}\left|\sum_j \exp(i\omega_{M2} t_j)\right|$$

If the sequence is perfectly periodic, the value is 1. Figure 2d shows the distribution of this normalized Fourier spectrum amplitude.